pubs.acs.org/chemneuro

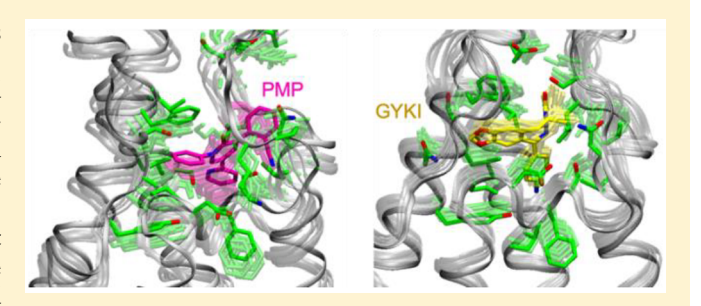
AMPA Receptor Noncompetitive Inhibitors Occupy a Promiscuous **Binding Site**

Chamali Narangoda, Serzhan N. Sakipov, and Maria G. Kurnikova*

Department of Chemistry, Carnegie Mellon University, Pittsburgh, Pennsylvania 15213, United States

Supporting Information

ABSTRACT: Noncompetitive inhibitors of AMPA receptors have attracted interest in recent years as antiepileptic drugs. However, their development is hindered by a lack of detailed understanding of the protein-inhibitor interaction mechanisms. Recently, structures of AMPA receptor complexes with the structurally dissimilar, noncompetitive, small-molecule inhibitors pyridone perampanel (PMP), GYKI 53655 (GYKI), and CP 465022 (CP) were resolved, revealing that all three share a common binding site. However, due to the low resolution of the ligands, their exact binding modes and protein-ligand interactions remain ambiguous and insuffi-



ciently detailed. We carried out molecular dynamics (MD) simulations on X-ray-resolved and docked AMPA receptor complexes, including thermodynamic integration (TI) to compute ligand binding constants, in order to investigate the inhibitor binding modes in detail and identify key protein-ligand interaction mechanisms. Our analysis and simulations show that the ligand binding pocket at the interface of the receptor's transmembrane domain exhibits features also found in the binding pockets of the multidrug-resistance proteins. The inhibitors bind to such promiscuous pockets by forming multiple weak contacts, while the large, flexible pocket undergoes adjustments to accommodate structurally different ligands in different orientations. TI was able to identify a specific more favorable binding mode for GYKI, while PMP, which has a symmetric ring structure, produced several comparable poses indicating that it may bind in several orientations.

KEYWORDS: AMPA receptors, noncompetitive inhibitors, molecular dynamics simulations, perampanel, GYKI 53655, CP 465022

INTRODUCTION

AMPA-subtype ionotropic glutamate receptors (iGluRs) initiate the majority of fast excitatory synaptic transmission in the brain. Consequently, they play a key role in the development of epilepsy and the spread of seizures. Inhibitors of AMPA receptors have thus attracted significant interest in recent years as antiepileptic drugs.^{2,3} The most potent and selective inhibitors of AMPA receptors act via a noncompetitive mechanism. While a considerable number of small molecules that belong to various structural classes have been identified and tested as AMPA receptor noncompetitive antagonists, 4-8 thus far pyridone perampanel (PMP) is the only compound that has been clinically approved as an antiepileptic drug. 9,10 However, PMP still causes side effects at higher doses. 11,12 In order to develop safer and more effective drugs, a detailed understanding of the biochemical mechanism underlying noncompetitive inhibition is of extreme importance.

Until fairly recently, information on noncompetitive inhibition of AMPA receptors remained limited to kinetics and potency studies and identification of a few animo acid residues that affect inhibition via mutagenesis. 7,13-16 The recent determination of X-ray crystal structures of the rat AMPA-subtype GluA2 receptor complexes of noncompetitive antagonists GYKI 53655 (GYKI), CP 465022 (CP), and PMP

(see Figure S10 for chemical structures) provided new significantly more detailed structural information on noncompetitive inhibitor binding.¹⁷ The crystal structures reveal that these structurally dissimilar inhibitors bind to four equivalent binding sites located at the interface between the transmembrane domain (TMD) and linkers connecting the TMD to the ligand-binding domain (LBD) of each of the four subunits of the receptor (Figure S1A). While the receptor in crystal structures is in a closed conformation, studies indicate that GYKI and PMP bind to the active channel as well. 18,19 While the channel loses its 4-fold symmetry in the open state, two of the four binding sites retain a conformation similar to that of the closed channel. 20,21 Thus, the binding of the inhibitors to the active state is likely similar. However, due to their limited resolution, the crystal structures do not provide a detailed atomistic picture of specific protein-ligand interactions or even an exact orientation of the ligands at the binding pocket. While details of noncompetitive inhibition are not yet thoroughly understood, inhibitors are thought to act by serving as "wedges" between the transmembrane segments of the receptor to interrupt gating movements necessary for

Received: June 18, 2019 Accepted: October 9, 2019 Published: October 9, 2019



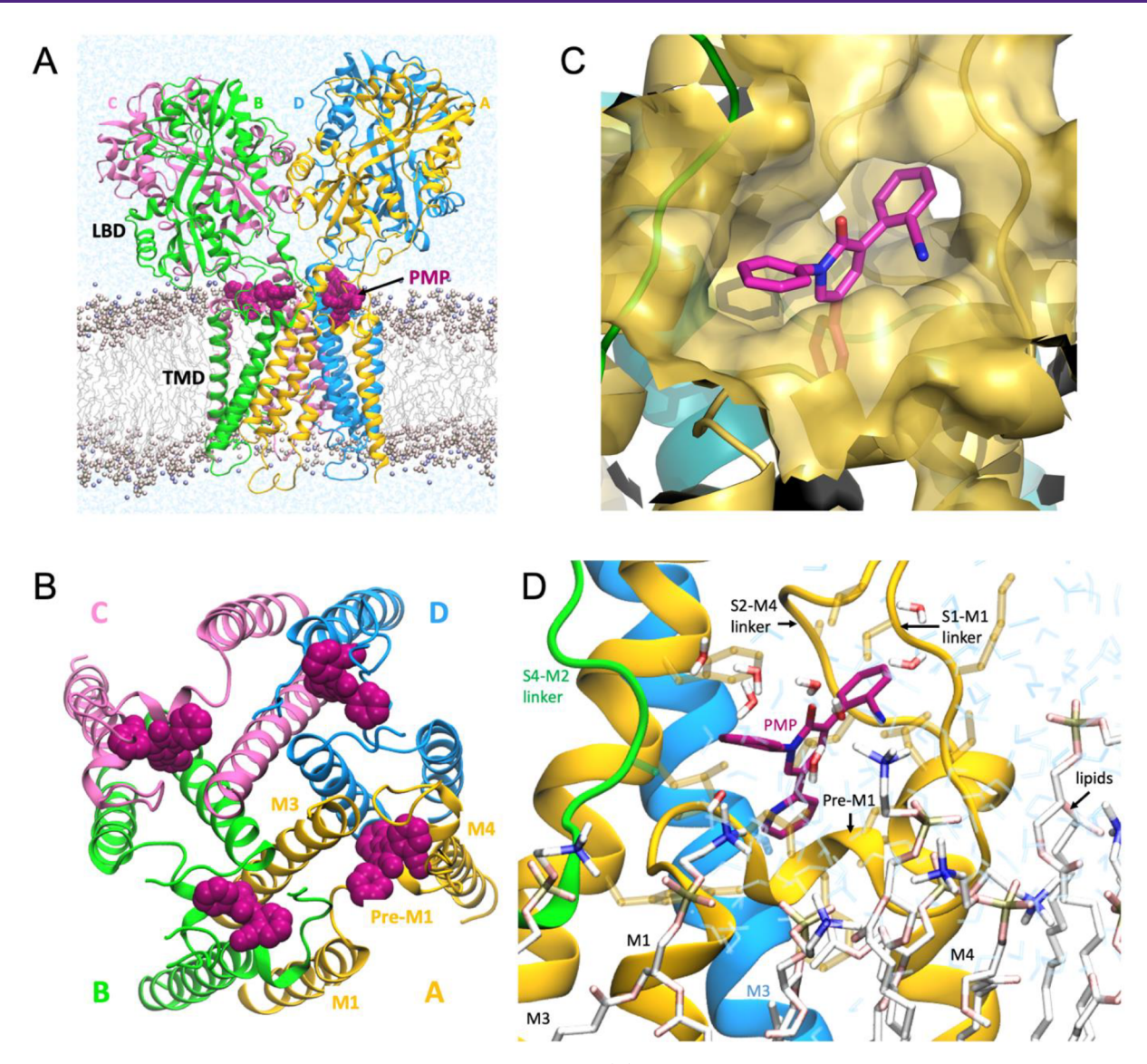


Figure 1. Simulated AMPA receptor TMD and LBD in complex of PMP. (A) Simulated system in POPC lipid membrane and water. Starting structure was PDB: 5L1F. Protein subunits are shown in different colors in cartoon representation. The four bound PMP inhibitors are shown in magenta in a space-filling representation. Some lipids and waters are removed for clarity. (B) Top view of simulated PMP binding sites. TMD and TMD-LBD linkers of the receptor and four bound PMP ligands are shown. (C) Surface view of the simulated PMP binding site in subunit A. (D) Close up view of the simulated PMP binding site in subunit A in a lipid membrane. PMP is shown as magenta in licorice representation. Receptor segments of different subunits are shown in different colors. Waters in the binding site within 4 Å of PMP are shown in licorice representation. Bulk water is shown as blue lines.

channel opening. ^{17,20} However, the shortage of information on the nature of protein—ligand interactions at the binding site is a significant limitation to gaining a better understanding of how these inhibitors exert their effect. Although these antagonists share a common binding pocket, receptor mutagenesis studies carried out on GYKI, ^{15,17} PMP, ¹⁷ and CP¹⁵ complexes of AMPA receptors have indicated that individual protein residues contribute differently to the binding of different ligands. Identifying significant features of the binding pocket that contribute to the binding of these antagonists will be key to successful rational design of the next generation of small molecule inhibitors that target AMPA receptors.

To develop a detailed understanding of biochemical determinants of small molecule binding and inhibition of the AMPA receptor, we carried out a comprehensive molecular

modeling study of GYKI, PMP, and CP ligand interactions with the receptor in a nearly native environment, including lipid bilayer and water solution. Our combined molecular docking, molecular dynamics (MD) simulations, and binding free energy calculations help assess the stability of crystallographically determined binding modes and explore other potential binding modes of GYKI, PMP, and CP. Moreover, our MD studies highlight the features of the AMPA receptor noncompetitive inhibitor binding site that are important in accommodating structurally different inhibitors. This information will aid in structure-based design of new noncompetitive inhibitors that target AMPA receptors, as well as other drug targets that share similar features such as multidrug-binding pockets.

RESULTS AND DISCUSSION

MD Simulations of the TMD and LBD of the AMPA Receptor Complex with PMP. The crystal structures of AMPA receptor-inhibitor complexes (PDBs: 5L1H, 5L1F, and 5L1E) and previous mutagenesis studies reveal a number of residues that line the binding pocket that are likely to contribute to noncompetitive inhibitor binding. 15,17 These include residues in pre-M1 (S516, F517, D519, P520), M3 (S615, Y616, L620, F623), and M4 (N791) helices of the receptor, and one residue in the S2-M4 linker (S788) (see Figures 1 and 5 for the locations of these residues). To obtain a detailed atomistic picture of inhibitor binding in a near-native environment, we carried out 800 ns of MD simulations of the PMP bound AMPA receptor TMD and LBD domains in a POPC lipid bilayer and water. The simulation provides information on dynamics of inhibitor binding and enables us to characterize the binding pocket in further detail. The simulated system is shown in Figure 1 and Movie S1. The four binding pockets are large, flexible, partially water filled cavities in the extracellular collar of the ion channel, a region that is important and undergoes significant structural changes during gating 18 (Figure 1C and D). The pockets are located near the lipid-water interface and open to the extracellular solution. Ligands only interact with residues in the TMD and the TMD-LBD linkers and do not interact with the LBD or lipids. Residues from pre-M1 helix and extracellular portions of M3 and M4 helices form a largely hydrophobic region of the pocket. However, pre-M1 and TMD-LBD linkers contain a number of polar and charged residues that come in close contact with ligands. In the original crystal structure, the four binding sites are nearly identical, though close examination reveals slight differences in interactions with the four bound ligands (Tables S1, S2, and S4). In the MD simulation, these differences become more pronounced, mainly due to the flexibility of the TMD-LBD linkers (Movies S2-S5). The flexible linkers make the pocket less structured compared to the original crystal structure. As a result, each ligand interacts somewhat differently with the receptor. While PMP remains stable in the binding site, interactions with PMP are mostly weak contacts that are broken and formed during the course of the simulation (Figure S2). The dynamic position of the inhibitor in the pocket is consistent with the low resolution of crystal structures. Interactions of ligands with TMD-LBD linkers are also more prominent in the simulated structure compared to the original crystal structure. The S2-M4 linker in particular shows significant flexibility and can be shared by two adjacent pockets, simultaneously interacting with two ligands (Movies S2-S5).

MD Simulations of Truncated AMPA Receptor Complexes with Inhibitors. The low resolution of crystal structures and the promiscuous nature of binding observed in our MD simulations raise the question of whether alternative binding modes exist for these noncompetitive inhibitors. To investigate other probable binding modes, we carried out a series of 100 ns simulations of crystal and docked AMPA receptor complexes with PMP, GYKI, and CP. Since inhibitors do not interact with the LBD, these simulations were performed on truncated systems that included only the TMD and TMD-LBD linkers loosely restrained at their ends (Figure S1B) to maximize computational efficiency in simulating a large number of poses. Simulated crystal complexes of PMP in the truncated system show comparable

behavior to the TMD-LBD system. Molecular docking produced alternative poses for all three ligands that showed comparable stability to crystal structure poses in MD simulations (Figures S3 and S4). Again, this is not surprising given the large size, flexibility, and chemical composition of the binding pocket. We assessed the stability of simulated poses using several measures: positional stability of the ligand (Figure S6), stability of the binding site (Figure S7), protein—ligand contacts and hydrogen bonds formed (Tables S1, S2 and S4), and ligand binding free energies (Tables 1, 2,

Table 1. Docking Scores and Binding Free Energies of PMP $Poses^a$

binding pose	docking score	MM-PBSA	TI
crystal			
PMPA	N/A	-29.34	-14.62
PMPB	N/A	-27.7	-13.54
PMPC	N/A	-32.34	-21.6
PMPD	N/A	-23.78	-14.13
docked			
PMP1A	-11.3	-28.69	-21.71
PMP1B	-9.1	-29.06	-20.95
PMP1C	-11.3	-28.7	-16.75
PMP1D	-10.3	-29.85	-7.74
PMP2A	-10.6	-17.01	-10.21
PMP2B	-9.3	-27.7	-4.54
PMP2C	-9.4	-26.49	-11.77
PMP2D	-10.3	-29.38	-11.78
a 111	1 1 1 1	1-1	

^aAll energies are reported in kcal mol⁻¹.

Table 2. Docking Scores and Binding Free Energies of GYKI Poses^a

binding pose	docking score	MM-PBSA	TI
crystal			
GYKIA	N/A	-26.44	-46.54
GYKIB	N/A	-29.39	-19.24
GYKIC	N/A	-23.56	-11.82
GYKID	N/A	-21.57	N/A
docked			
GYKI1A	-9.5	-25.59	-45.41
GYKI1B	-8.3	-24.34	-44.57
GYKI1C	-8.2	-23.09	N/A
GYKI1D	-9.2	-27.24	-14.81
GYKI2A	-9	-21.32	N/A
GYKI2B	-8.6	-31.59	-21.6
GYKI2C	-8.4	-28.14	-19.98
GYKI2D	- 7	-24.71	N/A
a All anaraias ara	concerted in keel mo	1 -1	

^aAll energies are reported in kcal mol⁻¹.

and S3). Most poses form multiple contacts and a few hydrogen bonds with binding site residues. Similar to the case of the simulation of the TMD-LBD complex of PMP, the binding poses of a given ligand with very similar orientations (the four poses from the original crystal of a given ligand, for example) show some variation in their specific interactions with the protein in simulations (Figures S3—S5 and Tables S1, S2, and S4). Unless otherwise stated, trajectory analysis and binding free energy calculations using Molecular Mechanics Poisson—Boltzmann Surface Area (MM-PBSA) (Tables 1, 2 and S3) and Molecular Mechanics Generalized-Born Surface Area (MM-GBSA) (results not shown) methods were

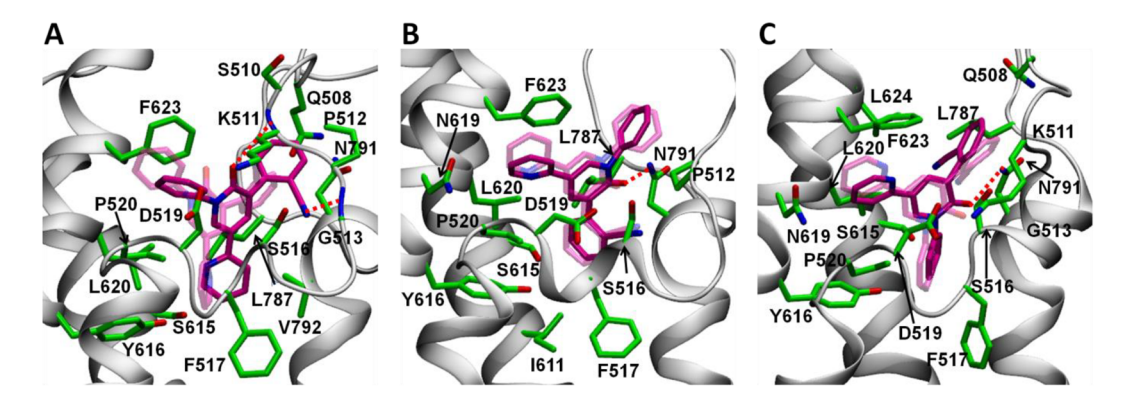


Figure 2. Stable PMP poses with the lowest binding energies. (A) PMPC (crystal), (B) PMP1A (docked), and (C) PMP1C (docked). Simulated representative structure (opaque) is superimposed on the initial minimized structure using stable helical parts of the corresponding subunit. Initial position of the protein is not shown. Initial ligand position is displayed (transparent). All residues within 4 Å of the ligand in the simulated structure are shown.

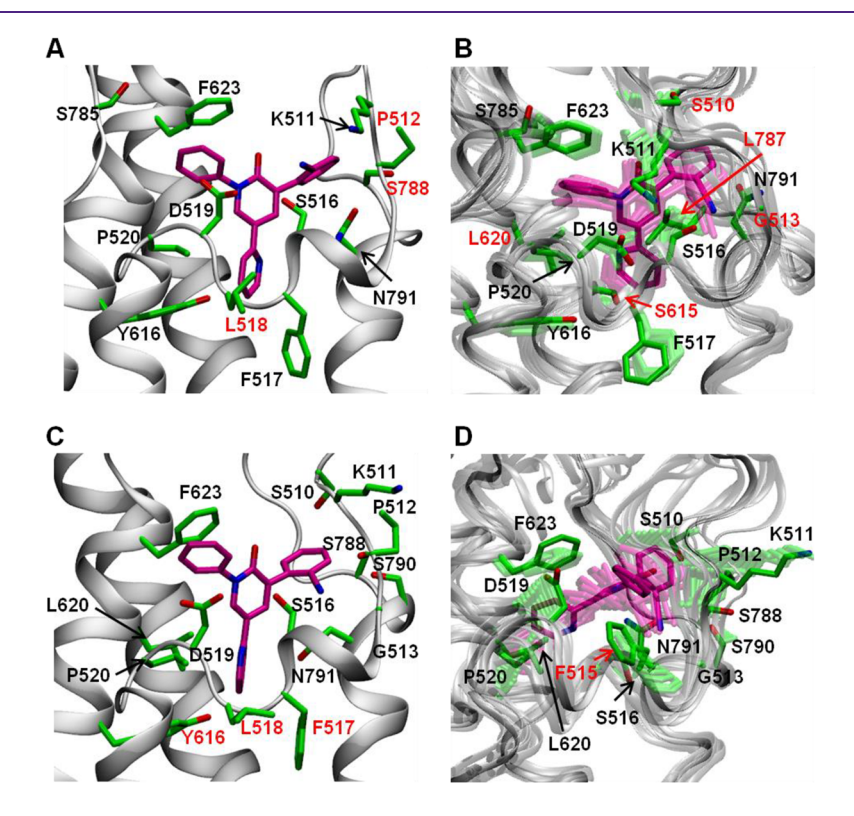


Figure 3. Initial (left) and simulated (right) conformations of crystal structure pose PMPA (A, B) and docked pose PMP1B (C, D). All residues within 4 Å of the ligand in each pose are shown. Contacts lost/gained during simulations are labeled in red. (A) Initial pose of PMPA after minimization. (B) Simulated trajectory of PMPA. Representative simulated pose (opaque) is overlapped with 10 snapshots that show the evolution of the trajectory in the final 25 ns of simulation (transparent). (C) Initial pose of PMP1B after minimization. (D) Simulated trajectory of PMPB. Representative simulated pose (opaque) is overlapped with 10 snapshots that show the evolution of the trajectory in the final 25 ns of simulation (transparent).

performed on a stable 25 ns portion of each MD trajectory. While end point free energy methods such as MM-PBSA and MM-GBSA have been successfully used to calculate binding affinities and predict binding modes of ligands, ^{22–24} these methods do not significantly discriminate between simulated crystal and docked poses of AMPA receptor inhibitors. The same features that contribute to ligand promiscuity of the binding site allow ligands to form favorable contacts with the pocket in several orientations, making it more difficult to discriminate between closely related binding modes. We used thermodynamic integration (TI) as a more discriminatory

approach to calculate binding free energies of all PMP poses and several GYKI poses. MD simulation results of crystal and docked complexes of PMP and GYKI are discussed in the following sections. (A more detailed description of specific interactions of PMP and GYKI poses and MD simulation results of CP is included in the Supporting Information.)

Binding Modes of PMP. Simulated binding poses of PMP are shown in Figure S3. The X-ray crystal structure of PMP was resolved at 4.0 Å, a lower resolution than that of GYKI. The symmetric ring structure of PMP also makes the ligand position in the binding pocket more ambiguous compared to

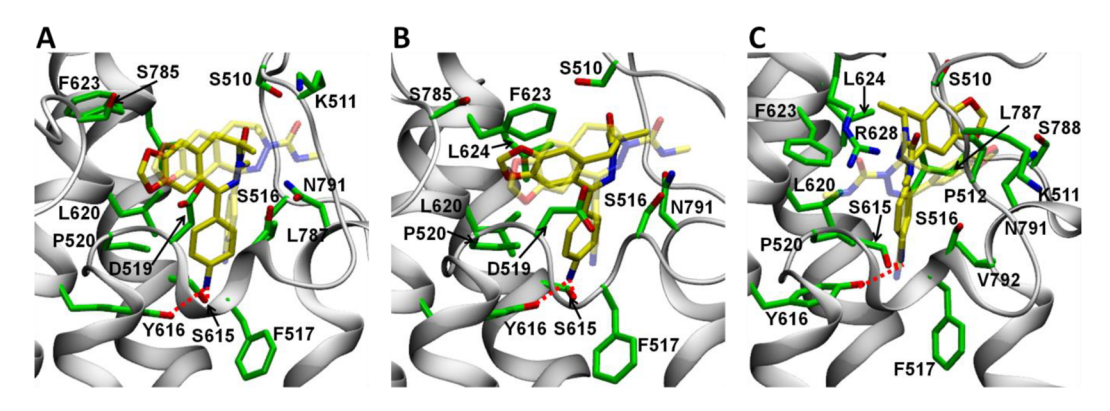


Figure 4. Orientations of GYKI. (A) GYKIB (crystal structure), (B) GYKI1A (docked in crystal-like orientation). (C) GYKI2B (docked in "flipped" orientation). Simulated representative structure (opaque) is superimposed on initial minimized structure using stable helical parts of the corresponding subunit. Initial position of the protein is not shown. Initial ligand position is displayed (transparent). All residues within 4 Å of the ligand in the simulated structure are shown.

GYKI and CP. Unsurprisingly, docking of PMP resulted in the highest number of alternative binding modes. PMP docked in four other global orientations in addition to the one reported in the crystal structure (Figures 2 and S3). Note that global orientation is loosely defined based on the orientation of outer aromatic rings of PMP; if specific protein-ligand interactions are considered there is even more variation among PMP binding poses. Docking scores of PMP poses also fall within a narrower range than that of GYKI and CP (see Table 1). All PMP poses except two remained stable during MD simulations. The exceptions are PMP1B and PMP2A, both docked poses, which became unstable during simulations resulting in destabilization of the binding pocket (see Figures S3 and S7). Figure 3 shows snapshots from the simulated trajectory of PMP1B in comparison with the stable, well behaved trajectory of PMPA. MM-PBSA (Table 1) and MM-GBSA (not shown) energies do not discriminate significantly between the rest of the poses.

Results of PMP simulations are summarized in Table S1. Although PMP binds in various orientations, most poses interact with a similar set of receptor residues. A majority of initial contacts in the PMP crystal poses are maintained throughout the simulations, although initial hydrogen bonds are not maintained. However, ligand functional groups and protein residues that participate in hydrogen bonding remain the same among simulated crystal and docked PMP poses. Carbonyl and nitrile groups of PMP are the main groups that participate in hydrogen bonding. While both groups serve as hydrogen bond acceptors, carbonyl group forms stronger and more stable hydrogen bonds.

Overall, hydrogen bond forming residues in simulated poses are S510, K511, G513, and N791. The main binding site residues that remain in contact with PMP in all poses are K511, S516, F517, D519, P520, Y616, L620, F623, N791, and S615 of the adjacent subunit. Previous mutagenesis studies found that residues S516, F517, P520, S615, F623, and N791 contribute to binding of PMP, which is consistent with these results. Additionally, residues S510, P512, G513, N619, L624, L787, V792, and S785 of the neighboring subunit, also form close contacts with PMP in some binding poses. These results are further supported by the TI results which did not provide a conclusive division between the poses. There is little to no correlation between TI and MM-PBSA/GBSA results as well as TI energies among the poses (see Figure S8A). Binding

free energies computed using TI method favor simulated crystal poses in general, with PMPC having the lowest energy among all poses (Table 1). Out of the docked poses that remained stable in MD simulations, PMP1A and PMP1C, each with a global orientation different from that of the crystal structure poses, show binding free energies comparable to simulated crystal poses (see Table 1 and Figure 2).

Binding Modes of GYKI. All simulated binding poses of GYKI are shown in Figure S4, and simulation results are summarized in Table S2. GYKI has the best resolution among crystal structures at 3.8 Å. ¹⁷ Docking of GYKI resulted in two distinct binding modes: one with the same orientation as the pose reported in the crystal structure (GYKI1A-1D) and the other with a "flipped" conformation (GYKI2A-2D). The crystal-like binding pose produced by docking is equivalent to the crystal pose in terms of binding energies and interactions formed. The flipped conformation docked to the same position, overlapping with the crystal structure pose, but shifted toward the S2-M4 linker during MD simulations. Examples of the two orientations of GYKI are shown in Figure 4. In the following discussion, original crystal and crystal-like docked poses are referred to as group 1 poses (as in Figure 4A and B) and flipped poses are referred to as group 2 poses (as in Figure 4C). On average, the two binding modes show comparable docking scores and MM-GBSA/PBSA binding free energies and similar average ligand RMSDs (see Tables 2 and S2). Due to their overlap in position, the two poses also form similar contacts at the binding site.

Two main hydrogen bonds involving aminophenyl nitrogen of GYKI are consistent among both group 1 and group 2 poses. The NH₂ group acts has a hydrogen bond donor, donating both its hydrogens to form two hydrogen bonds with the side chain OH groups of S615 of the neighboring subunit and Y616 of M3. These two hydrogen bonds are maintained through the course of MD simulations in the majority of GYKI poses. The amide nitrogen of the side chain of N791 forms unstable hydrogen bonds with either or both ring nitrogens of GYKI in all simulated crystal poses (Figure S4 and Table S2). In general, both group 1 and group 2 form contacts with a common set of binding site residues. Residues S510, K511, S516, F517, D519, P520, S615 (adjacent subunit), Y616, L620, F623, L624, L877, and N791 form contacts with GYKI in the majority of simulated poses. These interactions formed by GYKI are consistent with previous electrophysiological studies

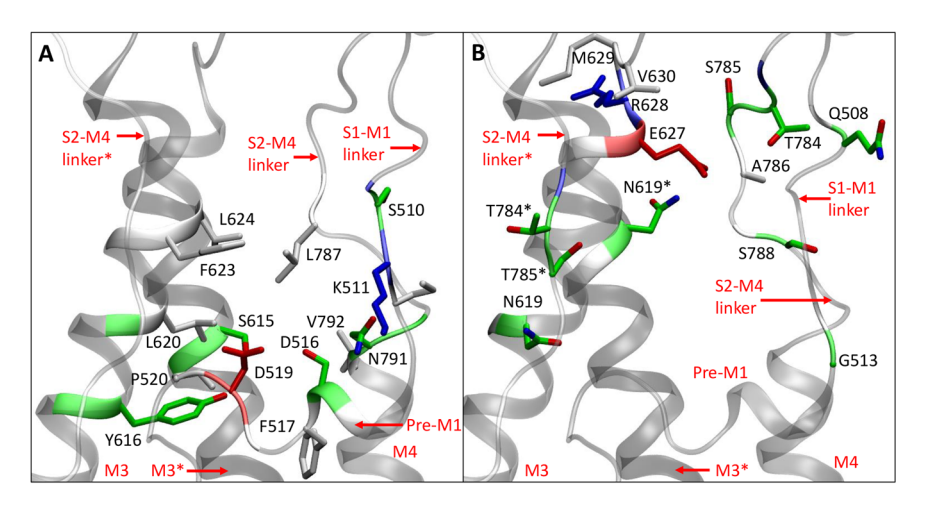


Figure 5. Interacting residues colored by type. (A) Residues interacting with most poses. These residues form contacts with 14 or more simulated poses of GYKI, PMP, and CP. (B) Residues interacting with some poses. These residues form contacts with two to eight simulated poses of GYKI, PMP, and CP. Residues are colored by type: polar (green), hydrophobic (purple), negatively charged (red), and positively charged (blue). (All residues that form contacts in two or more poses are shown.)

which attributed the binding of GYKI to residues S516, F517, P520, S615, F623, S788, and N791.¹⁷ In some poses, contacts are formed with additional residues in TMD-LBD linkers. Group 2 poses interact more strongly with the S2-M4 linker and are more likely to form contacts with residues T784, S785, A786, and S788, while in group 1 contacts with the S2-M4 linker appear to weaken during MD simulations. Both group 1 and group 2 poses are also consistent with the determined binding orientation via brominated GYKI in the crystal structures.¹⁷

In MD simulations of the group 1 poses, two distinct conformations of GYKI are observed. They differ by the presence or absence of a pucker in the diazepine ring of GYKI (compare Figure 4A and B and see Figure S4). TI free energies of binding for GYKI in these two conformations differ significantly, with puckered GYKI binding much more strongly to the binding site (see Table 2 poses GYKIA, GYKI1A, and GYKI1B). We performed quantum mechanical calculations of a stand-alone GYKI molecule in both conformations and found a negligible energy difference between them (on the order of less than 1 kT). Hence, the difference in the free energies found in TI simulations is due to GYKI binding with the receptor and not due to internal stress on the molecule due to the puckering. The contacts and hydrogen bonding are largely preserved between these two GYKI conformations but the side chain of F623 has a different orientation with regard to GYKI (see Figure 4A and B). It is worth noting that TI was able to distinguish between these binding modes, while MM-PBSA was not able to capture the difference (see Figure S3 and Table 2). This binding orientation is consistent with stronger inhibitory effect shown by GYKI 53655 in comparison to GYKI 52466 which lacks the 3-methylcarbamyl group. 18,25 Interaction of the 3-methylcarbamyl group with the S1-M1 and S2-M4 linkers likely enhances the binding of GYKI 53655.

Comparison of Calculated Binding Affinities with Experimental Values. While numerous studies report IC_{50} and K_d values for PMP, GYKI, and CP under various conditions, there is no reliable information on absolute binding affinities of these inhibitors. The following IC_{50} values were obtained for GluA2 inhibition by the three inhibitors in the original crystallographic study; $IC_{50} = 0.89 \ \mu M$ for PMP, $IC_{50} = 14.5 \ \mu M$ for GYKI, and $IC_{50} = 0.76 \ \mu M$ for CP. The IC_{50}

values reported in different studies range from 0.093 to 7.0 μM for PMP, $^{26-29}$ 1 to 34 μ M for GYKI, 13,15,18 and 0.015 to 0.3 μ M for CP.^{7,15} The significant differences in values are likely due to differences in experimental conditions and subunit composition of the receptor. However, these studies show that PMP and CP are more potent inhibitors of AMPA receptors compared to GYKI. This is in contradiction with the significantly lower TI binding free energies obtained for specific GYKI poses in comparison to PMP poses. In agreement with experiment, PMP and CP make more contacts with receptor residues (one more than GYKI on average) in our simulations and produce slightly lower MM-PBSA energies. However, the position of PMP and CP in the binding pocket fluctuates more compared to GYKI (see Figure S6). The higher number of closely related binding poses observed for these two ligands and the lower resolution of their X-ray derived structures further suggest the flexible nature of their binding. The stronger binding of PMP and CP is likely due to the entropic contribution from the flexible binding shown by these two ligands, which is not accounted for in the TI values as the binding energies were calculated for one representative structure of each pose. It is worth noting that although TI values reported here are useful in distinguishing between closely related poses of a given inhibitor, they do not represent absolute binding affinities of the inhibitors.

Promiscuity of the Binding Pocket. Our 100 ns atomistic MD simulations of 36 binding poses, including the 12 ligands in original X-ray crystal complexes and 24 additional docked poses, highlight the features that make the noncompetitive inhibitor binding site of the AMPA receptor promiscuous, allowing it to accommodate structurally dissimilar ligands in different orientations. Figure 5 shows binding site residues that form close contacts with ligands in simulated crystal and docked poses. Each individual inhibitor interacts mainly with residues from pre-M1, M3, M4, and TMD-LBD linkers of a single subunit, along with a few residues in the M3 helix of one of the neighboring subunits, and sometimes residues in the S2-M4 linker of the other adjacent subunit. While inhibitors do not directly interact with each another, the S2-M4 linker is often shared by two adjacent pockets. Thus, it may be possible that the binding of one ligand may affect the binding of another ligand to an adjacent pocket. Several amino

acid residues consistently contribute to the binding of different inhibitors, or different conformations of the same inhibitor (Figure 5A), while other residues contribute to varying degrees depending on the inhibitor and/or orientation (Figure 5B). Residues S516, D519 (pre-M1), L620, F623 (M3), N791 (M4), and S615 (M3 of the neighboring subunit) form close contacts with ligands in almost all binding poses of all three inhibitors, out of which a contact with F623 is present in all 36 poses. S615 is the main residue from a neighboring subunit that contributes to binding in most simulated crystal and docked conformations. Other residues that form contacts with ligands in a majority of poses are S510, K511 (S1-M1 linker), F517, P520 (pre-M1), Y616, L624 (M3), and L787 (S2-M4 linker). Residues P512 (pre-M1), V792 (M4) and S785 (S2-M4 linker) also form contacts with ligands in more than 10 binding poses. Residues that consistently participate in hydrogen bonding with ligands in various poses are S510, K511, G513, S516 (S1-M1 linker/pre-M1), S615 (M3 of the neighboring subunit), Y616 (M3), and N791 (M4). However, most hydrogen bonds formed are not persistent. Aromatic residues that remain in close proximity to ligands (F623, F517, and in some cases Y616) are also likely to interact with ligands by forming $\pi - \pi$ interactions. Similar features are found in binding sites of multidrug-resistance proteins, which accommodate a variety of structurally different ligands. 30,31 These proteins also contain large, flexible binding pockets that are characterized by the presence of multiple aromatic residues and hydrogen bond donor and acceptor sites.

Interaction of Inhibitors with TMD-LBD Linkers. Most of the receptor residues that interact with inhibitors simulated poses are in contact with inhibitors in initial X-ray crystal structures and consistent with previous electrophysiological studies. However, S1-M1 and S2-M4 linkers show significant flexibility in MD simulations and residues in these linkers, including some that do not appear to be part of the binding pocket in the original X-ray structures, interact with ligands and sometimes participate in hydrogen bonding. These linkers undergo significant conformational changes in gating. In addition to contacts with S510 and K511 in the S1-M1 linker which are present in the majority of poses, S785 in the S2-M4 linker forms contacts with ligands in a number of poses. Residues Q508, S784, A786, and S788 also form contacts with ligands in some poses (Figure 5B).

A few residues in the M3-S2 linker also interact with ligands in MD simulations. While the four binding sites are equivalent in the closed state of the receptor, the channel loses its 4-fold symmetry at residue E627 of the M3 helix and adopts different conformations in diagonal subunits A/C and B/D (Figure S9). Although most simulated poses do not interact with this region of the channel, some, mostly CP poses and some GYKI poses, come in contact with one or more of the residues F627, R628, M629, and V630. These contacts are not present in X-ray derived crystal structures. Poses in which a contact with at least one of the above residues is present are GYKIA, GYKID, GYKI2B, GYKI2C, CPA, CPB, CPC, CPD, CP1D, CP2A, CP2C, and CP2D (Tables S2 and S4). PMP in subunit B of the TMD-LBD simulation also forms contacts with the S2-M3 linker (Movie S3). This is worth noting since previous mutagenesis studies suggest that this region is involved in AMPA receptor gating.

The flexibility of the TMD-LBD linkers and pre-M1 helix allows the binding pocket to adapt to facilitate the binding of different ligands in various orientations, indicating that binding

of different ligands is likely accomplished through an inducedfit mechanism. As an example, panels A and B in Figure 6 each

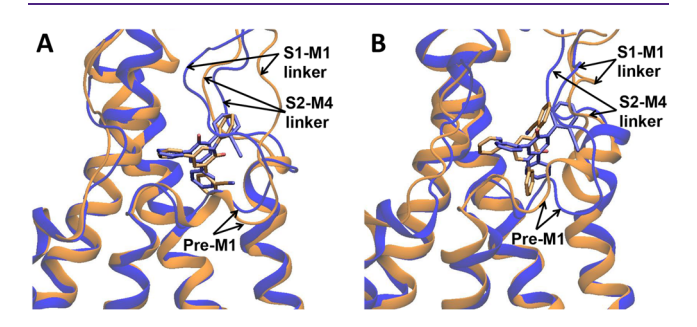


Figure 6. Adjustment of the binding pocket to accommodate different poses. Overlap of representative simulated structures of (A) PMPA (crystal, blue) and PMP1A (docked, orange) and (B) PMPC (crystal, blue) and PMP1C (docked, orange) is shown. Flexibility of the S1-M1 and S2-M4 linkers and pre-M1 region allows the binding pocket to adapt to facilitate the binding of different ligands in various orientations.

show the overlap of two simulated poses with favorable TI binding energies with the same initial protein configuration (i.e., same binding site) and different ligand orientations. Pre-M1 and linker regions undergo adjustments during MD simulations to favorably accommodate the different binding modes. As discussed in the preceding sections, such variations in interactions due to pocket flexibility are also present to a considerable degree among poses with similar orientations, including simulated crystal structure poses. Variations in ligand position and contacts in similar poses with comparable binding free energies support the idea that inhibitors bind by forming multiple weak interactions with protein residues, allowing for some movement of the ligand within the binding pocket. An example of such a rearrangement from the TMD-LBD simulation of PMP is illustrated in Figure 7; PMP in the

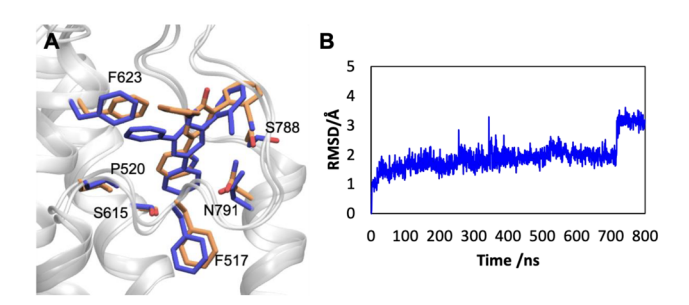


Figure 7. Rearrangement of PMP in binding site D. (A) PMP in the binding site in subunit D of TMD-LBD simulation undergoes a shift in position around 716.5 ns, while the binding site does not undergo significant change. PMP at 716 ns is shown in blue. PMP at 716.5 is shown in orange. (B) Ligand RMSD of PMP in binding site D. The change in RMSD around 716.5 ns corresponds to rearrangement of PMP in the binding site.

binding site in subunit D undergoes a shift in ligand position around 716 ns of the simulation, moving toward the S1-M1 linker and remaining stable in its new position.

The flexibility shown by the TMD-LBD linkers is an important finding in this study. These linkers undergo major conformational changes in gating, and their interaction with inhibitors in MD simulations (Figure 5) suggests that the

inhibitors may stabilize them in closed conformation. Comparison of our results with previous studies also indicates that the linkers, particularly S1-M1 and S2-M4, may contribute significantly to inhibitor binding. As an example, the 3methylcarbamyl group of GYKI, which forms interactions with some residues of these linkers in its most favorable binding mode, is known to contribute to its potency. 18,25 Additionally, introducing larger groups such as heterocyclic ring systems to the N-3 position of GYKI compounds was shown to improve their potency.³³ This is likely due to interactions with the S1-M1 and S2-M4 linkers resulting in stronger binding. However, in MD simulations, we observe that PMP, GYKI, and CP only interact with residues in these linkers sporadically to varying degrees (Figure 5B). Thus, introducing functional groups to generate stronger, more stable interactions with S1-M1 and S2-M4 linkers may further enhance the binding of inhibitors to this pocket. These linkers contain a number of charged polar residues that are capable of forming hydrogen bonds and interacting with polar groups in ligands.

In conclusion, extensive simulations of three noncompetitive inhibitors that all bind in the same general binding site at the water interface of the TMD domains reveal stability and mobility of the binding site and the inhibitor molecules within it. Crystal structure poses of all three inhibitors undergo some adjustments but remain stable during MD simulations. All crystal-like bound poses produced favorable binding free energies. Moreover, all three inhibitors also produced alternative binding modes that remain stable during MD simulations. PMP produced several comparable binding modes with favorable binding free energies, indicating that PMP may bind in several orientations. While GYKI docked in two crystal-like and flipped orientations, computing its free energy of binding allowed us to distinguish a specific binding mode. The main finding of our study is that the interfacial TMD binding site is promiscuous and capable of accommodating multiple ligands in a variety of poses. The ambiguity of the binding site may be compared to binding sites in multidrug resistance proteins, which are characterized by multiple aromatic residues flanking the large binding site with multiple hydrogen bond donor and acceptor sites that can accommodate transient interactions with a variety of ligands.³¹ All inhibitors form multiple weak interactions with the binding site protein residues, forming a number of hydrophobic contacts and hydrogen bonds. Short time scale switching of proteinligand contacts within the binding pocket indicate a dynamic ligand binding position, which is consistent with the relatively low resolution of all ligands in the X-ray derived structures. The Pre-M1 and linker regions of the binding pocket undergo adjustments to accommodate structurally different ligands in different orientations. Receptor-ligand interactions observed are consistent with previous mutagenesis studies. 15,17 However, due to the flexibility of the pocket, inhibitors interact with residues in the TMD-LBD linkers that do not appear to be part of the binding pocket in the X-ray crystal structures. Particularly, we find that the S1-M1 and S2-M4 linkers, which had not previously been identified as part of the binding pocket, show significant flexibility and interact with inhibitors. We suggest that introducing polar functional group that interact with these linkers is likely to improve the binding of inhibitors to this pocket.

METHODS

Molecular Docking. X-ray crystal structures of AMPA receptors in complex with GYKI (PDB: 5L1H), PMP (PDB: 5L1F), and CP (PDB: 5L1E) were used as starting structures for all docking and MD simulations. ¹⁷ Original cocrystallized ligands were removed from the crystal structure complexes, and docking of GYKI, PMP, and CP to corresponding AMPA receptors was performed using AutoDock Vina.³⁴ Each ligand was optimized in Gaussian09 using the B3LYP density functional theory method with the 6-31G basis set prior to docking.35 AutoDockTools was used to prepare the ligands and receptors for docking.³⁶ Docking was done to each binding site (A-D) separately. Two rounds of docking were performed for each ligand: (a) rigid docking with no rotatable bonds in either the protein or the ligand and (b) docking with one to three rotatable bonds in the ligand. For each ligand, eight of the lowest energy poses generated were chosen for MD simulations. Binding poses were selected so that they represent different orientations of the ligand as well as the lowest binding energies.

Simulation Details. The TMD and LBD of AMPA receptor complex of PMP (PDB: 5L1F) and truncated systems of crystal and docked complexes of PMP, GYKI, and CP containing only the TMD and TMD-LBD linkers were simulated. For each ligand, three truncated TMD systems containing a total of 12 binding poses (original X-ray crystal structure containing four original cocrystallized ligands and two more systems each containing four docked ligands) were simulated. All protein—ligand complexes were inserted into preequilibrated membranes of POPC lipids and solvated with water and neutralizing ions. TMD-LBD complex of PMP contained approximately 31×10^4 atoms including 1632 protein resides, four ligands, 483 POPC lipids, and 73400 waters and neutralizing ions. A truncated TMD system contained approximately 92×10^3 atoms including 572 protein residues, four ligands, 240 POPC lipids, and approximately 17000 waters and neutralizing ions.

All MD simulations were carried out with AMBER 14³⁷ or AMBER 16³⁸ using PMEMD on GPU cards. The FF99SB-ILDN³⁹ force field was used in combination with the general AMBER force field (GAFF)⁴⁰ for ligands, Amber Lipid14⁴¹ force field for lipids and TIP3P⁴² for water. Parameters for ligands were created using Antechamber.⁴³ A simulation time step of 2 fs was used and all hydrogen bonds were constrained via SHAKE. 44 Periodic boundary conditions were applied in all directions with a cutoff radius of 10 Å. Electrostatic interaction calculations were performed using Particle Mesh Ewald (PME) method. 45 Langevin thermostat and Berendsen barostat, 46 as implemented in AMBER, were used to maintain temperature and pressure, respectively. All simulations were carried out in the NPT ensemble using anisotropic scaling available in GPU accelerated PMEMD. Each system was equilibrated at 1 atm and 300 K with gradually decreasing harmonic restraints on the protein and ligands over 60 ns for the TMD-LBD system and 12 ns for truncated TMD systems. Production simulations were carried out for approximately 800 ns for the TMD-LBD system and 100 ns for TMD systems. The simulation protocol is described in detail in the Supporting Information.

Analysis of Trajectories. Simulations were monitored by calculating the root-mean-square deviation (RMSD) of the protein $C\alpha$ atoms as a function of time with respect to starting position. In all systems protein RMSD reached to around 3-4 Å and stabilized within 5-10 ns of unrestrained simulations. In order to evaluate the positional stability of ligands while accounting for the flexibility of the pocket, we computed an RMSD of selected ligand atoms with respect to their initial contacts. Namely, the ligand RMSD reported is the root-mean-square deviation of distances between selected ligandatoms and binding site residue-atoms in close proximity to the ligand as shown and described in Figure S11 and Table S11. The RMSD of the residues aligning the binding pocket was calculated to assess the stability of the pocket (Figure S7). All analyses of simulated poses and MM-GBSA/PBSA binding energy calculations were performed on 25 ns of a stable portion of the trajectory. A representative structure of each binding pose during this analysis period was used as starting

structure for TI calculations. Residues that remained within 4 Å of a ligand for over 60% of the analysis period were considered to be in contact with the ligand in its simulated pose. RMSD and hydrogen bond analyses were carried out using cpptraj module in AmberTools. MM-GBSA/PBSA free energy calculations were carried out using scripts included in AMBER and AmberTools. Visual Molecular Dynamics (VMD)⁴⁷ was used to visualize trajectories and create images.

Thermodynamic Integration and ab Initio Quantum **Mechanics Calculations.** The thermodynamic integration (TI) method was applied to calculate the free energies of ligand binding in simulated poses. AMBER PMEMD TT^{48} implementation was used in this study. To make the TI calculations feasible, we performed them in truncated systems for each ligand pose in a single binding pocket individually. Each truncated ligand-protein binding pocket system was a cut-out of the full simulated system and consisted of a ligand, truncated protein, water, and lipids within 15 Å of the ligand and placed in a box of ca. 7000 explicit water molecules. The free energy difference of the protein system in the presence and the absence of a ligand was then computed by gradually vanishing the ligand from the binding pocket in 12 λ steps. Production simulations were done for 10 ns for each λ . The reported free energies are $\Delta G = \Delta G_{\text{prot}} - \Delta G_{\text{wat}}$ where ΔG_{prot} is the free energy of introducing a ligand in the binding site and ΔG_{wat} is the free energy of solvation of the ligand in a pure water. TI simulations to compute ΔG_{wat} were performed using the same protocol as described above, with the ligand initially placed in a box of ca. 2000 water molecules.

Quantum mechanical (QM) calculations were performed to compare energies of two GYKI conformations, which occurred during MD simulations. These were performed using the Gaussian software package.³⁵ For structure optimization, a density functional theory (DFT) method was used as implemented in Gaussian with the B3LYP functional and 6-311G+(d,p) basis set. A final single point energy was computed using DFT optimized structures using the MP2 method and the same basis set.

ASSOCIATED CONTENT

S Supporting Information

The Supporting Information is available free of charge on the ACS Publications website at DOI: 10.1021/acschemneur-o.9b00344.

Additional results and methods: Truncated TMD simulation setup; RMSD plots from TMD-LBD simulation; supplementary docking and MD simulation results; RMSD plots from truncated TMD simulations; correlation between TI and MM-PBSA free energies; M3-S2 linker in diagonal subunits; chemical structures of Inhibitors; MD simulation protocol; calculation of ligand "RMSD" (PDF)

Movie S1: Trajectory of PMP (magenta) in the binding pockets. Protein residues within 10 Å from PMP are shown as green (polar), gray (hydrophobic), red (negatively charged), and blue (positively charged) surfaces. Movies S2–S5: Trajectory of PMP (magenta) and interacting residues in binding sites in subunits A (Movie S2), B (Movie S3), C (Movie S4), and D (Movie S5). Residues are colored by segment: pre-M1/M1 (violet), M3/M3-S2 linker (cyan), M4/S2-M4 linker (yellow), M3 of neighboring subunit (orange), M4/S2-M4 linker of neighboring subunit (green) (ZIP)

AUTHOR INFORMATION

ORCID ®

Chamali Narangoda: 0000-0001-6786-3992 Serzhan N. Sakipov: 0000-0001-7414-4670 Maria G. Kurnikova: 0000-0002-8010-8374

Author Contributions

C.N. carried out docking and MD simulations, analyzed and interpreted data, and contributed to manuscript writing; S.N.S. performed TI calculations, analyzed and interpreted data, and contributed to manuscript writing; M.G.K. designed the project, interpreted data, and contributed to manuscript writing.

Funding

This work was supported by the NIH Grant R01NS083660, and in part by the NSF Grant DMP15629. This work used the Extreme Science and Engineering Discovery Environment (XSEDE), which is supported by National Science Foundation grant number ACI-1548562. Specifically, it used the Bridges system, which is supported by NSF award number ACI-1445606, at the Pittsburgh Supercomputing Center (PSC).

Notes

The authors declare no competing financial interest.

ACKNOWLEDGMENTS

The authors would like to thank A. Sobolevsky for introducing us to the problem, expert advice, and critical reading of the manuscript.

REFERENCES

- (1) Traynelis, S. F., Wollmuth, L. P., McBain, C. J., Menniti, F. S., Vance, K. M., Ogden, K. K., Hansen, K. B., Yuan, H., Myers, S. J., and Dingledine, R. (2010) Glutamate receptor ion channels: structure, regulation, and function. *Pharmacol. Rev.* 62 (3), 405–496.
- (2) Meldrum, B. S., and Rogawski, M. A. (2007) Molecular targets for antiepileptic drug development. *Neurotherapeutics* 4 (1), 18–61.
- (3) Rogawski, M. A. (2011) Revisiting AMPA Receptors as an Antiepileptic Drug Target: Revisiting AMPA Receptors as an Antiepileptic Drug Target. *Epilepsy Currents* 11 (2), 56–63.
- (4) Donevan, S. D., and Rogawski, M. A. (1993) GYKI 52466, a 2, 3-benzodiazepine, is a highly selective, noncompetitive antagonist of AMPA/kainate receptor responses. *Neuron* 10 (1), 51–59.
- (5) Hibi, S., Ueno, K., Nagato, S., Kawano, K., Ito, K., Norimine, Y., Takenaka, O., Hanada, T., and Yonaga, M. (2012) Discovery of 2-(2-oxo-1-phenyl-5-pyridin-2-yl-1, 2-dihydropyridin-3-yl) benzonitrile (perampanel): a novel, noncompetitive α -amino-3-hydroxy-5-methyl-4-isoxazolepropanoic acid (AMPA) receptor antagonist. *J. Med. Chem.* 55 (23), 10584–10600.
- (6) Donevan, S. D., Yamaguchi, S.-i., and Rogawski, M. A. (1994) Non-N-methyl-D-aspartate receptor antagonism by 3-N-substituted 2, 3-benzodiazepines: relationship to anticonvulsant activity. *J. Pharmacol. Exp. Ther.* 271 (1), 25–29.
- (7) Lazzaro, J. T., Paternain, A. V., Lerma, J., Chenard, B. L., Ewing, F. E., Huang, J., Welch, W. M., Ganong, A. H., and Menniti, F. S. (2002) Functional characterization of CP-465, 022, a selective, noncompetitive AMPA receptor antagonist. *Neuropharmacology* 42 (2), 143–153.
- (8) Niu, L. (2015) Mechanism-based design of 2, 3-benzodiazepine inhibitors for AMPA receptors. *Acta Pharm. Sin. B* 5 (6), 500–505.
- (9) Patsalos, P. N. (2015) The clinical pharmacology profile of the new antiepileptic drug perampanel: a novel noncompetitive AMPA receptor antagonist. *Epilepsia 56* (1), 12–27.
- (10) Steinhoff, B. J. (2015) The AMPA receptor antagonist perampanel in the adjunctive treatment of partial-onset seizures: clinical trial evidence and experience. *Ther. Adv. Neurol. Disord.* 8 (3), 137–147.
- (11) Juhl, S., and Rubboli, G. (2017) Add-on perampanel and aggressive behaviour in severe drug-resistant focal epilepsies. *Funct. Neurol.* 32 (4), 215.
- (12) Rugg-Gunn, F. (2014) Adverse effects and safety profile of perampanel: a review of pooled data. *Epilepsia* 55, 13–15.

(13) Donevan, S., and Rogawski, M. A. (1998) Allosteric regulation of α -amino-3-hydroxy-5-methyl-4-isoxazole-propionate receptors by thiocyanate and cyclothiazide at a common modulatory site distinct from that of 2, 3-benzodiazepines. *Neuroscience* 87 (3), 615–629.

- (14) Menniti, F. S., Chenard, B. L., Collins, M. B., Ducat, M. F., Elliott, M. L., Ewing, F. E., Huang, J. I., Kelly, K. A., Lazzaro, J. T., and Pagnozzi, M. J. (2000) Characterization of the binding site for a novel class of noncompetitive α -amino-3-hydroxy-5-methyl-4-isoxazolepropionic acid receptor antagonists. *Mol. Pharmacol.* 58 (6), 1310–1317.
- (15) Balannik, V., Menniti, F. S., Paternain, A. V., Lerma, J., and Stern-Bach, Y. (2005) Molecular mechanism of AMPA receptor noncompetitive antagonism. *Neuron* 48 (2), 279–288.
- (16) Wang, C., Wu, A., Shen, Y.-C., Ettari, R., Grasso, S., and Niu, L. (2015) Mechanism and Site of Inhibition of AMPA Receptors: Substitution of One and Two Methyl Groups at the 4-Aminophenyl Ring of 2, 3-Benzodiazepine and Implications in the "E" Site. ACS Chem. Neurosci. 6 (8), 1371–1378.
- (17) Yelshanskaya, M. V., Singh, A. K., Sampson, J. M., Narangoda, C., Kurnikova, M., and Sobolevsky, A. I. (2016) Structural bases of noncompetitive inhibition of AMPA-subtype ionotropic glutamate receptors by antiepileptic drugs. *Neuron 91* (6), 1305–1315.
- (18) Shi, E. Y., Yuan, C. L., Sipple, M. T., Srinivasan, J., Ptak, C. P., Oswald, R. E., and Nowak, L. M. (2019) Noncompetitive antagonists induce cooperative AMPA receptor channel gating. *J. Gen. Physiol.* 151 (2), 156–173.
- (19) Yuan, C. L., Shi, E. Y., Srinivasan, J., Ptak, C. P., Oswald, R. E., and Nowak, L. M. (2019) Modulation of AMPA receptor gating by the anticonvulsant drug, Perampanel. ACS Med. Chem. Lett. 10 (3), 237–242.
- (20) Yelshanskaya, M. V., Mesbahi-Vasey, S., Kurnikova, M. G., and Sobolevsky, A. I. (2017) Role of the ion channel extracellular collar in AMPA receptor gating. *Sci. Rep.* 7 (1), 1050.
- (21) Twomey, E. C., Yelshanskaya, M. V., Grassucci, R. A., Frank, J., and Sobolevsky, A. I. (2017) Channel opening and gating mechanism in AMPA-subtype glutamate receptors. *Nature* 549 (7670), 60.
- (22) Hou, T., Wang, J., Li, Y., and Wang, W. (2011) Assessing the performance of the MM/PBSA and MM/GBSA methods. 1. The accuracy of binding free energy calculations based on molecular dynamics simulations. *J. Chem. Inf. Model.* 51 (1), 69–82.
- (23) Genheden, S., and Ryde, U. (2015) The MM/PBSA and MM/GBSA methods to estimate ligand-binding affinities. *Expert Opin. Drug Discovery* 10 (5), 449–461.
- (24) Greenidge, P. A., Kramer, C., Mozziconacci, J.-C., and Sherman, W. (2014) Improving docking results via reranking of ensembles of ligand poses in multiple X-ray protein conformations with MM-GBSA. J. Chem. Inf. Model. 54 (10), 2697–2717.
- (25) Kapus, G. L., Gacsályi, I., Vegh, M., Kompagne, H., Hegedüs, E., Leveleki, C., Hársing, L. G., Barkóczy, J., Bilkei-Gorzó, A., and Lévay, G. (2008) Antagonism of AMPA receptors produces anxiolytic-like behavior in rodents: effects of GYKI 52466 and its novel analogues. *Psychopharmacology* 198 (2), 231–241.
- (26) Hanada, T., Hashizume, Y., Tokuhara, N., Takenaka, O., Kohmura, N., Ogasawara, A., Hatakeyama, S., Ohgoh, M., Ueno, M., and Nishizawa, Y. (2011) Perampanel: a novel, orally active, noncompetitive AMPA-receptor antagonist that reduces seizure activity in rodent models of epilepsy. *Epilepsia* 52 (7), 1331–1340.
- (27) Zwart, R., Sher, E., Ping, X., Jin, X., Sims, J., Chappell, A., Gleason, S., Hahn, P., Gardinier, K., and Gernert, D. (2014) Perampanel, an antagonist of α -amino-3-hydroxy-5-methyl-4-isoxazolepropionic acid receptors, for the treatment of epilepsy: studies in human epileptic brain and nonepileptic brain and in rodent models. *J. Pharmacol. Exp. Ther.* 351 (1), 124–133.
- (28) Ceolin, L., Bortolotto, Z. A., Bannister, N., Collingridge, G. L., Lodge, D., and Volianskis, A. (2012) A novel anti-epileptic agent, perampanel, selectively inhibits AMPA receptor-mediated synaptic transmission in the hippocampus. *Neurochem. Int.* 61 (4), 517–522.
- (29) Barygin, O. I. (2016) Inhibition of calcium-permeable and calcium-impermeable AMPA receptors by perampanel in rat brain neurons. *Neurosci. Lett.* 633, 146–151.

- (30) Kumar, N., Radhakrishnan, A., Wright, C. C., Chou, T. H., Lei, H. T., Bolla, J. R., Tringides, M. L., Rajashankar, K. R., Su, C. C., Purdy, G. E., et al. (2014) Crystal structure of the transcriptional regulator Rv1219c of Mycobacterium tuberculosis. *Protein Sci.* 23 (4), 423–432.
- (31) Wong, K., Ma, J., Rothnie, A., Biggin, P. C., and Kerr, I. D. (2014) Towards understanding promiscuity in multidrug efflux pumps. *Trends Biochem. Sci.* 39 (1), 8–16.
- (32) Yelshansky, M. V., Sobolevsky, A. I., Jatzke, C., and Wollmuth, L. P. (2004) Block of AMPA receptor desensitization by a point mutation outside the ligand-binding domain. *J. Neurosci.* 24 (20), 4728–4736.
- (33) Wang, C., Han, Y., Wu, A., Sólyom, S. n., and Niu, L. (2014) Mechanism and site of inhibition of AMPA receptors: pairing a thiadiazole with a 2, 3-benzodiazepine scaffold. *ACS Chem. Neurosci.* 5 (2), 138–147.
- (34) Trott, O., and Olson, A. J. (2010) AutoDock Vina: improving the speed and accuracy of docking with a new scoring function, efficient optimization, and multithreading. *J. Comput. Chem.* 31 (2), 455–461.
- (35) Frisch, M., Trucks, G., Schlegel, H. B., Scuseria, G., Robb, M., Cheeseman, J., Scalmani, G., Barone, V., Mennucci, B., and Petersson, G. et al. (2009) *Gaussian 09*, revision a.02, Gaussian. Inc., Wallingford, CT.
- (36) Morris, G. M., Huey, R., Lindstrom, W., Sanner, M. F., Belew, R. K., Goodsell, D. S., and Olson, A. J. (2009) AutoDock4 and AutoDockTools4: Automated docking with selective receptor flexibility. *J. Comput. Chem.* 30 (16), 2785–2791.
- (37) Case, D. A., Babin, V., Berryman, J. T., Betz, R. M., Cai, Q., Cerutti, D.S., Cheatham, T.E., III, Darden, T. A., Duke, R. E., Gohlke, H., Goetz, A. W., Gusarov, S., Homeyer, N., Janowski, P., Kaus, J., Kolossváry, I., Kovalenko, A., Lee, T. S., LeGrand, S., Luchko, T., Luo, R., Madej, B., Merz, K. M., Paesani, F., Roe, D. R., Roitberg, A., Sagui, C., Salomon-Ferrer, R., Seabra, G., Simmerling, C. L., Smith, W., Swails, J., Walker, R. C., Wang, J., Wolf, R. M., Wu, X., and Kollman, P. A. (2014) *AMBER 14*, University of California, San Francisco.
- (38) Case, D. A., Betz, R. M., Cerutti, D.S., Cheatham, T. E., III, Darden, T. A., Duke, R. E., Giese, T. J., Gohlke, H., Goetz, A. W., Homeyer, N., Izadi, S., Janowski, P., Kaus, J., Kovalenko, A., Lee, T. S., LeGrand, S., Li, P., Lin, C., Luchko, T., Luo, R., Madej, B., Mermelstein, D., Merz, K. M., Monard, G., Nguyen, H., Nguyen, H. T., Omelyan, I., Onufriev, A., Roe, D. R., Roitberg, A., Sagui, C., Simmerling, C. L., Botello-Smith, W. M., Swails, J., Walker, R. C., Wang, J., Wolf, R. M., Wu, X., Xiao, L., and Kollman, P. A. (2016) AMBER 16. University of California, San Francisco.
- (39) Lindorff-Larsen, K., Piana, S., Palmo, K., Maragakis, P., Klepeis, J. L., Dror, R. O., and Shaw, D. E. (2010) Improved side-chain torsion potentials for the Amber ff99SB protein force field. *Proteins: Struct., Funct., Genet.* 78 (8), 1950–1958.
- (40) Wang, J., Wolf, R. M., Caldwell, J. W., Kollman, P. A., and Case, D. A. (2004) Development and testing of a general amber force field. *J. Comput. Chem.* 25 (9), 1157–1174.
- (41) Dickson, C. J., Madej, B. D., Skjevik, Å. A., Betz, R. M., Teigen, K., Gould, I. R., and Walker, R. C. (2014) Lipid14: the amber lipid force field. *J. Chem. Theory Comput.* 10 (2), 865–879.
- (42) Jorgensen, W. L., Chandrasekhar, J., Madura, J. D., Impey, R. W., and Klein, M. L. (1983) Comparison of simple potential functions for simulating liquid water. *J. Chem. Phys.* 79 (2), 926–935.
- (43) Wang, J., Wang, W., Kollman, P. A., and Case, D. A. (2006) Automatic atom type and bond type perception in molecular mechanical calculations. *J. Mol. Graphics Modell.* 25 (2), 247–260.
- (44) Ryckaert, J.-P., Ciccotti, G., and Berendsen, H. J. (1977) Numerical integration of the cartesian equations of motion of a system with constraints: molecular dynamics of n-alkanes. *J. Comput. Phys.* 23 (3), 327–341.
- (45) Darden, T., York, D., and Pedersen, L. (1993) Particle mesh Ewald: An N· log (N) method for Ewald sums in large systems. *J. Chem. Phys.* 98 (12), 10089–10092.

(46) Berendsen, H. J., Postma, J. v., van Gunsteren, W. F., DiNola, A., and Haak, J. (1984) Molecular dynamics with coupling to an external bath. *J. Chem. Phys.* 81 (8), 3684–3690.

- (47) Humphrey, W., Dalke, A., and Schulten, K. (1996) VMD: visual molecular dynamics. *J. Mol. Graphics* 14 (1), 33–38.
- (48) Kaus, J. W., Pierce, L. T., Walker, R. C., and McCammon, J. A. (2013) Improving the efficiency of free energy calculations in the amber molecular dynamics package. *J. Chem. Theory Comput.* 9 (9), 4131–4139.